JPEDAV (2008) 29:500–508
DOI: 10.1007/s11669-008-9389-6

The Heusler Phase $Ti_{25}(Fe_{50-x}Ni_x)Al_{25}$ ($0 \le x \le 50$); Structure and Constitution

Xinlin Yan, A. Grytsiv, P. Rogl, V. Pomjakushin, and M. Palm

(Submitted April 10, 2008; in revised form June 11, 2008)

Alloys with composition $Ti_{25}(Fe_{50-x}Ni_x)Al_{25}$ ($0 \le x \le 50$) were investigated employing electron probe microanalysis (EPMA) and X-ray powder diffraction (XPD). For $TiFe_2Al$, in situ neutron powder diffraction (ND) was used for the inspection of phase constitution covering the temperature range from 27 °C (300 K) to 1277 °C (1550 K). Combined Rietveld refinement of ND and XPD data for $TiFe_2Al$ revealed that Fe atoms occupy the 8*c* site in space group $Fm\bar{3}m$, Ti with a small amount of Al sharing the 4*a* site, and the remaining Ti and Al atoms adopting the 4*b* site. This structural model was successfully applied in the refinement of all alloys $Ti_{25}(Fe_{50-x}Ni_x)Al_{25}$ ($0 \le x \le 50$). Partial atom order exists on the Fe-rich side while complete order is observed for the Ni-rich side. Profiles recorded by in situ neutron powder diffraction for $TiFe_2Al$ in the range of investigated temperatures show two phases, namely Heusler phase and $MgZn_2$-type Laves phase. Diffraction peaks from the Heusler phase dominate the profiles at lower temperatures but at higher temperatures the $MgZn_2$-type Laves phase is the main phase. No CsCl-type phase was found in the alloy in the investigated temperature range. The thermal expansion coefficient of $TiFe_2Al$ is 1.4552×10^{-5} K^{-1}.

Keywords crystal chemistry, diffraction (X-ray/neutron powder), intermetallics, site occupancy, ternary and quaternary titanium aluminides, titanium-iron-nickel-aluminum alloy

1. Introduction

Since the first Heusler alloy was identified by Heusler[1] in 1903, intermetallic compounds with Heusler-type structure are attracting considerable interest due to their unique magnetic, mechanical, thermoelectric and other physical properties. FeAl-base and NiAl-base alloys with Heusler type are considered as potential high temperature structural materials with high strength in combination with excellent oxidation resistance.[2-8] It is well known that intermetallic alloys with CsCl-type structure, for example NiAl aluminides,[5-10] are important candidates for high temperature structural application. However, shortages exist such as poor ductility at room temperature and the loss of strength at high temperature because of the open structure of the ordered bcc lattice. Alloying with elements that form Heusler phase precipitates has been demonstrated as a useful way to solve this problem.[2,6,7,11-14] Particularly the control of the two-phase microstructure of the CsCl and the Heusler phases turned out to be very important.[5] Isopleths were established for the sections NiAl-$TiNi_2Al$,[5] FeAl-$TiFe_2Al$,[15] Fe_3Al-$TiFe_2Al$-FeAl,[16,17] NiAl-$TiNi_2Al$-TiNi,[15,18,19] $TiNi_2Al$-TiNi,[20] and (Fe, Ni)Al-Ti (Fe, Ni).[15] The influences of the replacement of X or Z in X_2YZ by a fourth element[15,21-23] on (i) the critical boundaries of the CsCl/Heusler phase, (ii) the transition temperature from Heusler to CsCl phase, and (iii) the stability of Heusler phase were well investigated and discussed.[24] The lattice misfit between the two coherent phases, CsCl and Heusler phase, was also thought to be an important factor to affect the mechanical properties by influencing the shape of the precipitates, the spatial distribution in the alloy and the coarsening behavior.[6,12,19,25,26] On the other hand, atom substitution in binary alloys can drastically increase the transition temperature to enlarge the range of the Heusler phase, specifically, in binary Fe_3Al with BiF_3-type structure and/or in ternary $MnCu_2Al$-type by substitution of Al by Si[27] or of Fe by M (M = Ti,[4,16] V, Cr, Mn, and Mo[26,28]), respectively. For the ternary alloys, $TiFe_2Al$ and $TiNi_2Al$, past efforts focused on physical properties,[3,8,11,12,29-31] lattice parameters,[6,19,32-40] and structure evaluations.[36] However, no investigation is known dealing with detailed atomic site preference in the Heusler phase of the quaternary system Ti-Fe-Ni-Al. Since the atom's environment in the unit cell (the atom species and position of the nearest neighbors) is of significance to the stability of the ordered phase[24] and to the material properties,[41] the present work provides detailed structural information for the Heusler phase in the quaternary system Ti-Fe-Ni-Al along the section $TiFe_2Al$-$TiNi_2Al$.

It is worthwhile to note the structural differences among the related structure types of W, CsCl, BiF_3, and $MnCu_2Al$. Figure 1 shows the crystal structures and corresponding simulated X-ray diffraction patterns with Miller indices for Ti-Fe-Al phases. For the structure type of W and CsCl, 8

Xinlin Yan, A. Grytsiv, and **P. Rogl,** Institute of Physical Chemistry, University of Vienna, Währingerstr. 42, A-1090 Wien, Austria; **V. Pomjakushin,** Laboratory for Neutron Scattering, ETH Zurich & Paul Scherrer Institut, CH-5232 Villigen PSI, Switzerland; **M. Palm,** Max-Planck Institut für Eisenforschung GmbH, Max-Planck-Str. 1, 40237 Düsseldorf, Germany. Contact e-mail: yanxinlin13@hotmail.com.

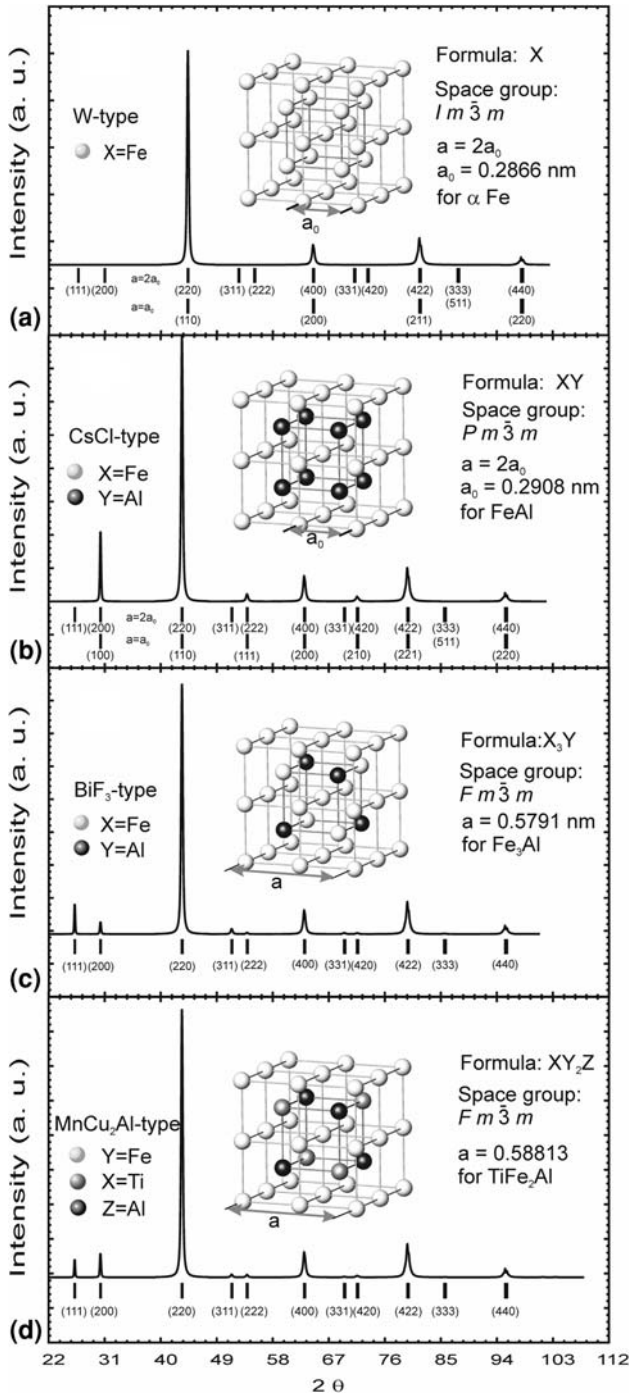

Fig. 1 Structure types of W (a), CsCl (b), BiF_3 (c), $MnCu_2Al$ and corresponding X-ray diffraction patterns simulated for Ti-Fe-Al alloys. For more convenient comparison, the origins of BiF_3 and $MnCu_2Al$-type unit cells have been shifted to (1/4, 1/4, 1/4) with respect to the conventional settings

conventional unit cells are used in Fig. 1(a) and (b) for convenient comparison with the larger cell of the BiF_3, and $MnCu_2Al$ types. Replacing the central atom in the W-type structure by an atom of a different species we arrive at the CsCl-type (Fig. 1b). As a consequence, the substitution changes the Bravais lattice from body-centered to primitive and thus triggers the appearance of "primitive" peaks in the diffraction patterns (e.g., (100) in the CsCl-cell corresponds to (200) in the unit cell with double lattice dimension; see Fig. 1b). The BiF_3 structure (formula X_3Y) consists of 8 W-type cells where 4 of the central atoms in tetrahedral position are replaced by a different element species all together revealing a face-centered symmetry (see Fig. 1c). The $MnCu_2Al$-type structure can be constructed by substitution of the second tetrahedral set of central atoms by a third atom species without reduction of the fcc symmetry (see Fig. 1d). Nonzero intensities of (111), (311) and (331) differentiate the Heusler type (BiF_3 and $MnCu_2Al$) from the CsCl-type (see Fig. 1b) but note that the Miller indices for the CsCl-type refer to a block of 8 conventional unit cells ($a = 2a_0$) in order to compare with the Heusler type).

2. Experimental Details

A series of alloys with nominal composition $Ti_{25}(Fe_{50-x}Ni_x)Al_{25}$ (x = 0, 10, 20, 25, 30, 40, and 50) were prepared by argon arc-melting, from high-purity materials (more than 99.9 mass%), on a water-cooled copper hearth. To insure homogenization, all alloys (1 g for each alloy) were re-melted three times. Part of each sample was vacuum sealed in quartz tubes and annealed at 900 °C for 10 days before being quenched in cold water. X-ray powder diffraction data from as-cast and annealed alloys were collected employing a Guinier-Huber image plate system with Cu-$K_{\alpha 1}$ or Fe-$K_{\alpha 1}$ ($8° < 2\theta < 100°$). Precise lattice parameters were calculated by least-squares fits to indexed 4θ-values employing Ge as internal standard (a_{Ge} = 0.5657906 nm). X-ray powder intensity data for the determination of structural parameters were collected on a Siemens D5000 instrument with Cu-$K_{\alpha 1,2}$ ($10° < 2\theta < 110°$, step (2θ) = 0.02°) equipped with an energy dispersive SOLX detector.

Neutron diffraction was performed at room temperature for the alloy $TiFe_2Al$ annealed at 900 °C in high intensity mode ($\Delta d/d \geq 2 \times 10^{-3}$) and on heating in the temperature range $27 \leq T \leq 1277$ °C ($300 \leq T \leq 1550$ K; heating rate: 5 °C/min and dwell time for diffraction run at isothermal temperature: 180 min) on the high-resolution HRPT diffractometer[42] at the SINQ spallation source of Paul Scherrer Institute, Switzerland. To reduce preferential orientation effects, the alloy was powdered to a grain size below 60 μm. The powder was contained in a Nb-can sealed under argon, the neutron wavelength is $\lambda_{neutron}$ = 0.1494 nm and the θ range was $5° \leq 2\theta \leq 165°$. After neutron diffraction the powder appeared to be densely sintered into a rod-shaped body that easily separated from the Nb-container. With respect to a possibly slow kinetic in reaching phase equilibrium during the relative short dwell time in neutron diffraction, discs were cut from the rod and were sealed individually and annealed at 800 °C for 10 days, 900 °C for 7 days, 1000 °C for 4 days, 1100 °C for 24 h and 1200 °C

for 12 h. After this long term annealing the phase constitutions in the discs were measured by XPD and EPMA and should insure equilibrium conditions.

Quantitative Rietveld refinement of the X-ray and neutron powder diffraction data was performed with the FULLPROF program,[43] employing internal tables for neutron scattering lengths and X-ray atomic form factors.

All as-cast and annealed samples were polished via standard procedures and have been examined by optical metallography and scanning electron microscopy (SEM). Specimen compositions were determined by Electron Probe Microanalysis (EPMA). Compositions of quaternary Ti-Fe-Ni-Al alloys were established on a Carl Zeiss DSM 962 instrument equipped with a link EDS system operated at 20 kV and 60 μA. Compositions of phases in the $TiFe_2Al$ alloy after ND and after annealing at various temperatures between 800 and 1200 °C have been measured on a Cameca SX 50 and a Jeol JXA-8100 at 15 kV and 20 nA using the pure elements as standards.

3. Results and Discussion

3.1 The Alloy Series $Ti_{25}(Fe_{50-x}Ni_x)Al_{25}$ ($0 \le x \le 50$)

X-ray diffraction patterns in Fig. 2(a) were collected from samples annealed at 900 °C with nominal compositions $Ti_{25}(Fe_{50-x}Ni_x)Al_{25}$ ($0 \le x \le 50$). In all cases a single Heusler-type structure was recorded except for $TiFe_2Al$, which besides the Heusler phase revealed a tiny amount of Laves phase, showing consistency with the phase diagram reported by Palm et al.[44,45] For 1000 °C a similar phase constitution was found by Fu et al.[41] in this alloy series. Lattice parameters a as a function of Ni content (x) are plotted in Fig. 3 in comparison with all literature data available for the Heusler-type phase. The small differences of lattice parameters for $Ti_{25}(Fe_{50-x}Ni_x)Al_{25}$ ($0 \le x \le 50$) are attributed to the comparable radii of Fe and Ni atoms.

As indicated in Fig. 1, the nonzero intensity of the (111) reflection is a strong evidence for the Heusler-type structure with respect to a CsCl or W-type structure (a detailed description of the characteristics of each structure type and corresponding X-ray powder diffractograms are presented in the Introduction). For $TiFe_2Al$, the weakness of the (111) XPD reflection prompted us to compare refinements for a CsCl-type with respect to a Heusler type. From the difference curves of the refinements (which yield close residual values for both structure types) in Fig. 2(b) it is not easy to recognize the proper structural type. However, the clearly exposed ND intensity of (111) compared to XPD and the significant difference for the (111) reflection in the Yobs.–Ycal. curves (see Fig. 2c) unambiguously indicated the Heusler type as the proper structure. The location of the heavy Fe atoms in the unit cell (8*c*-site) were easily defined by X-ray diffraction, while those of Ti can be found unambiguously by neutron diffraction due to the negative neutron scattering length of natural titanium. Therefore the combined Rietveld refinement of neutron and X-ray data for $TiFe_2Al$ clearly revealed: (i) Fe in the 8*c* positions, (ii) Ti

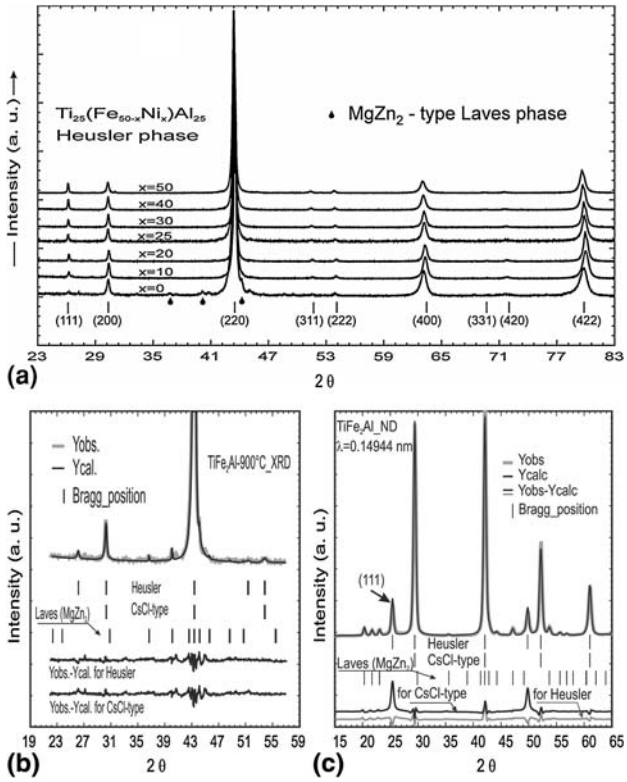

Fig. 2 Experimental X-ray diffraction patterns for the alloys $Ti_{25}(Fe_{50-x}Ni_x)Al_{25}$ ($0 \le x \le 50$) annealed at 900 °C (a) and Rietveld refinements for $TiFe_2Al$ from XPD (b) and ND (c) with respect to different structure types (for refinements with CsCl-type model, only the Yobs.–Ycal. curves and Bragg positions are presented in both cases)

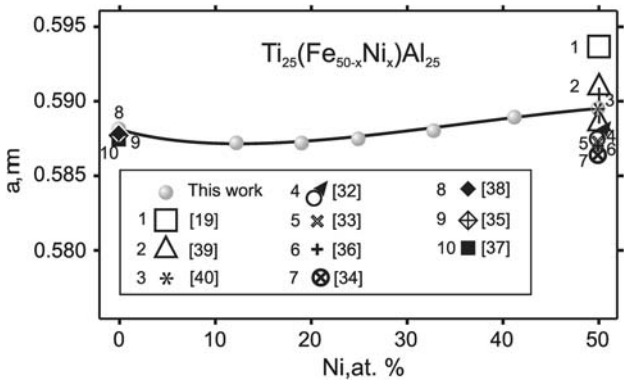

Fig. 3 Lattice parameters vs. Ni content in $Ti_{25}(Fe_{50-x}Ni_x)Al_{25}$ ($0 \le x \le 50$) (annealed at 900 °C) and comparison with literature data

atoms share with a small amount of Al the 4*a* sites and (iii) the remaining Ti and Al occupy the 4*b* sites. Due to centro-symmetry the intensity calculations with the 4*a* and 4*b* sites interchanged are equivalent, i.e., exchange of atom

Table 1 Structural data (Rietveld refinements, BiF_3, $Fm\bar{3}m$) for $Ti_{25}(Fe_{50-x}Ni_x)Al_{25}$ ($0 \le x \le 50$) compounds

Parameter/Compound	$Ti_{25}Fe_{50}Al_{25}$(a)	$Ti_{25}Fe_{40}Ni_{10}Al_{25}$	$Ti_{25}Fe_{30}Ni_{20}Al_{25}$	$Ti_{25}Fe_{25}Ni_{25}Al_{25}$
Composition from EMPA, at.%	$Ti_{23.8}Fe_{50.9}Al_{25.9}$	$Ti_{24.0}Fe_{38.4}Ni_{12.3}Al_{25.4}$	$Ti_{25.5}Fe_{32.4}Ni_{17.4}Al_{24.7}$	...
Composition from refinement, at.%	$Ti_{24.3}Fe_{50}Al_{25.7}$	$Ti_{24.5}(Fe,Ni)_{50}Al_{25.5}$	$Ti_{26.0}(Fe,Ni)_{50}Al_{24.0}$	$Ti_{26.4}(Fe,Ni)_{50}Al_{23.6}$
a, nm, Guinier	0.58813(1)	0.58716(4)	0.58719(7)	0.58747(4)
Reflections used in refinement	18/25	18	16	17
Number of variables	35	20	21	21
$R_F = \Sigma\lvert F_o - F_c\rvert / \Sigma F_o$	0.038/0.0090	0.049	0.028	0.041
$R_I = \Sigma\lvert I_o - I_c\rvert / \Sigma I_o$	0.053/0.0165	0.043	0.027	0.021
$R_{wP} = [\Sigma w_i\lvert y_{oi} - y_{ci}\rvert^2 / \Sigma w_i\lvert y_{oi}\rvert^2]^{1/2}$	0.113/0.042	0.072	0.064	0.053
$R_P = \Sigma\lvert y_{oi} - y_{ci}\rvert / \Sigma\lvert y_{oi}\rvert$	0.079/0.031	0.055	0.048	0.041
$R_e = [(N-P+C)/(\Sigma w_i y^2_{oi})]^{1/2}$	0.062/0.0048	0.042	0.047	0.045
$\chi^2 = (R_{wP}/R_e)^2$	3.29/75.9	2.97	1.86	1.36
M1, in 8c (1/4, 1/4, 1/4), Occ.	8.00Fe	8.00(Fe,Ni)	8.00(Fe,Ni)	8.00(Fe,Ni)
B_{eq} (B_{iso}) 10^2, nm^2	0.173(8)	0.65(3)	0.60(3)	0.71(4)
M2 in 4b (1/2, 1/2, 1/2), Occ.	0.30(1)Ti + 3.70Al	0.48(2)Ti + 3.52Al	0.43(2)Ti + 3.57Al	0.49(3)Ti + 3.51Al
B_{eq} (B_{iso}) 10^2, nm^2	0.34(2)	0.58(5)	0.44(6)	0.19(9)
M3 in 4a (0, 0, 0), Occ.	3.59(1)Ti + 0.41Al	3.44(2)Ti + 0.56Al	3.73(2)Ti + 0.27Al	3.74(3)Ti + 0.26Al
B_{eq} (B_{iso}) 10^2, nm^2	0.27(2)	0.48(4)	0.28(4)	0.69(7)
Secondary phase ($MgZn_2$-type Laves phase)	a = 0.4902 nm, c = 0.7954 nm	...	...	...

Parameter/Compound	$Ti_{25}Fe_{20}Ni_{30}Al_{25}$	$Ti_{25}Fe_{10}Ni_{40}Al_{25}$	$Ti_{25}Ni_{50}Al_{25}$
Composition from EMPA, at.%	$Ti_{23.9}Fe_{15.5}Ni_{34.9}Al_{25.7}$	$Ti_{24.1}Fe_{7.9}Ni_{42.2}Al_{25.8}$	$Ti_{24.5}Ni_{50.0}Al_{25.5}$
Composition from refinement, at.%	$Ti_{26.3}(Fe,Ni)_{50}Al_{23.7}$	$Ti_{25.0}(Fe,Ni)_{49.6}Al_{25.4}$	$Ti_{25.0}Ni_{50.4}Al_{24.6}$
a, nm, Guinier	0.58802(5)	0.58892(5)	0.58950(6)
Reflections used in refinement	16	17	18
Number of variables	21	21	21
$R_F = \Sigma\lvert F_o - F_c\rvert / \Sigma F_o$	0.044	0.032	0.030
$R_I = \Sigma\lvert I_o - I_c\rvert / \Sigma I_o$	0.030	0.016	0.016
$R_{wP} = [\Sigma w_i\lvert y_{oi} - y_{ci}\rvert^2 / \Sigma w_i\lvert y_{oi}\rvert^2]^{1/2}$	0.061	0.054	0.054
$R_P = \Sigma\lvert y_{oi} - y_{ci}\rvert / \Sigma\lvert y_{oi}\rvert$	0.046	0.041	0.039
$R_e = [(N-P+C)/(\Sigma w_i y^2_{oi})]^{1/2}$	0.038	0.032	0.026
$\chi^2 = (R_{wP}/R_e)^2$	2.53	2.92	4.31
M1, in 8c (1/4, 1/4, 1/4), Occ.	8.00(Fe,Ni)	8.00(Fe,Ni)	8.00Ni
B_{eq} (B_{iso}) 10^2, nm^2	0.61(2)	0.69(2)	0.59(3)
M2 in 4b (1/2, 1/2, 1/2), Occ.	0.42(2)Ti + 3.58Al	4.00Al	4.00Al
B_{eq} (B_{iso}) 10^2, nm^2	0.37(5)	0.20(5)	0.15(5)
M3 in 4a (0, 0, 0), Occ.	3.79(2)Ti + 0.21Al	4.00Ti	4.00Ti
B_{eq} (B_{iso}) 10^2, nm^2	0.28(4)	0.54(4)	0.54(4)
Secondary phase ($MgZn_2$-type Laves phase)	...	...	...

Data collection: D5000 (Cu-$K_{\alpha 1,2}$) and ND. Crystal structure data are standardized using the program Structure Tidy[46]
(a) Combined refinement of XPD/ND (λ_n = 0.1494 nm) data

occupation in these two positions does not influence the R-values in the Rietveld refinements. Although the deviation from a fully ordered Heusler-type atom arrangement is small, the random distribution significantly reduces $I_{(111)}$. This structure model was successfully employed on the other compounds of the alloy series $Ti_{25}(Fe_{50-x}Ni_x)Al_{25}$. All results from Rietveld refinements are summarized in Table 1. However, due to only slight differences for the X-ray scattering factors of Ni and Fe atoms, the occupation of Ni and Fe in the 8c site could not be defined, and therefore the Fe/Ni ratio was fixed from EPMA. The obvious increase of the intensity $I_{(111)}$ throughout the alloy series (as seen in Fig. 2a) corresponds to a monotonous decrease of the partial atom disorder in the 4a and 4b sites. Particularly for the alloys with $0 \le x \le 30$ (see Table 1 and Fig. 2), any attempts to attain more ordered arrangements failed yielding higher residual values or negative temperature factors (see Fig. 4). For x = 40 and 50, the 4a and 4b sites show full atom order in consistency with literature data.[36] It shall be noted that compositions derived from Rietveld refinements are in good agreement with nominal compositions as well as with the compositions obtained from EPMA (see Table 1).

3.2 In Situ Neutron Diffraction for $TiFe_2Al$ (RT < T < 1277 °C)

A sequence of plots of neutron diffraction patterns recorded for various temperatures for $TiFe_2Al$ are shown in Fig. 5. The corresponding reflections from the Laves phase and the Heusler phase as well as temperature axes were indicated and also those peaks that stem from the Nb-sample holder. Apparently, diffraction patterns from the Heusler phase dominated the profiles covering the temperature range from 27 °C (300 K) to 1027 °C (1300 K) (the profiles recorded at 1027 °C (1300 K) and 1077 °C (1350 K) were emphasized in Fig. 5 by a dashed line and a dotted line, respectively), while the $MgZn_2$-type Laves phase dominates above 1077 °C (1350 K). This indicates that at higher temperature the Laves phase is the main phase. Both cubic phases (Heusler or CsCl phase) and Laves phase coexist in the alloy at all the investigated temperatures. The presented profiles can not prove or reject visually the fact that the cubic phase is Heusler type or CsCl type at temperatures above 1077 °C. Although the characteristic peak (111) of the Heusler phase disappeared completely at about 1177 °C (1450 K), this cannot be taken as evidence that the CsCl-type phase appears, since the strongest peak (220) of the Heusler phase already was very weak. The characteristic peaks probably turned undetectable. Figure 6 shows the

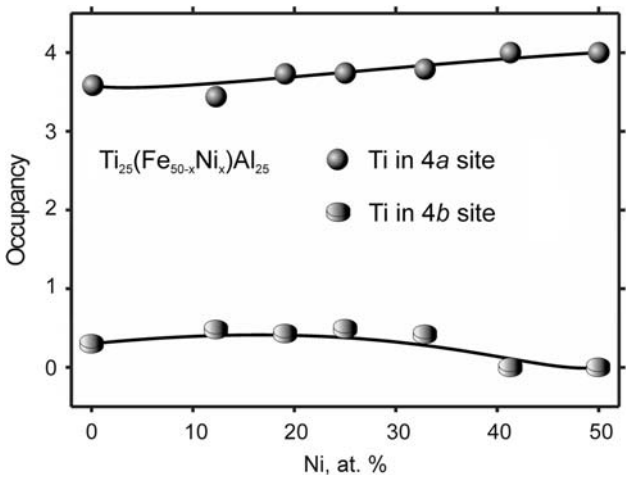

Fig. 4 Occupancy of Ti-atoms in 4*a* and 4*b* sites in $Ti_{25}(Fe_{50-x}Ni_x)Al_{25}$ ($0 \le x \le 50$) (annealed at 900 °C) vs. Ni content

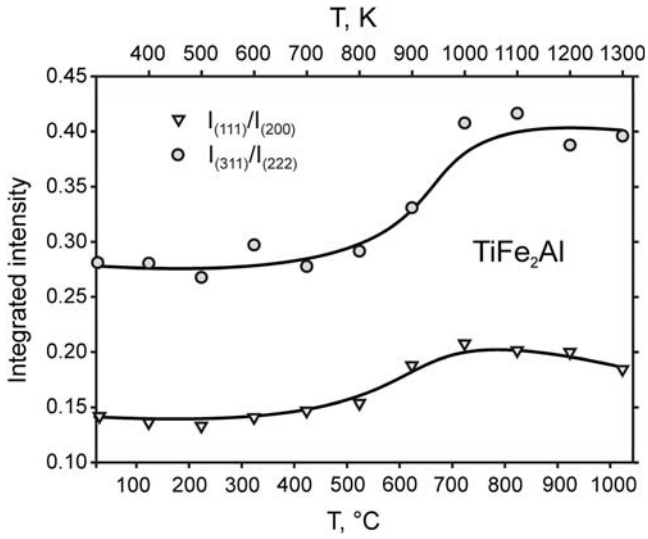

Fig. 6 Alloy $TiFe_2Al$. Neutron intensity ratio for the reflections (111)/(200) and (311)/(222) vs. temperature

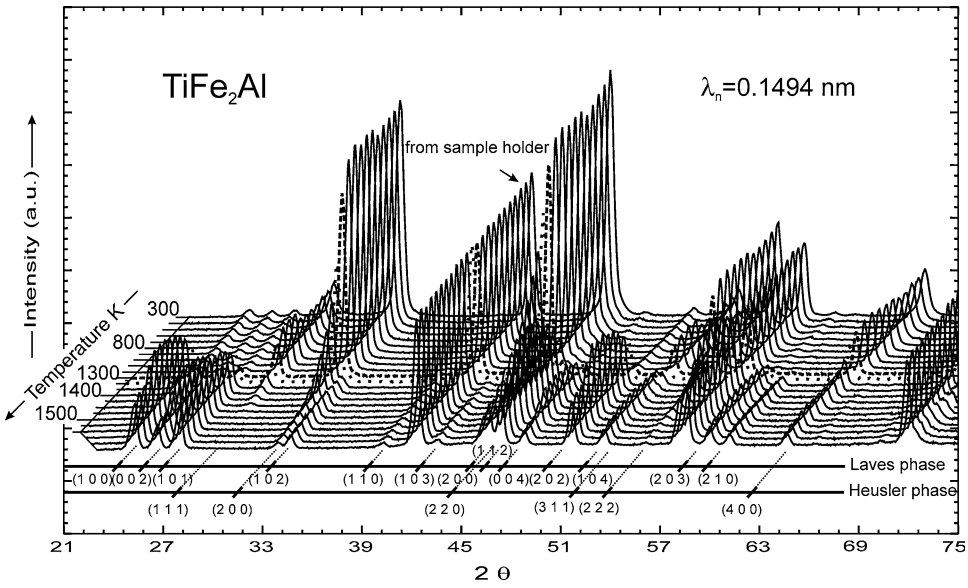

Fig. 5 Sequence of plots of neutron diffraction patterns recorded at various temperatures for $TiFe_2Al$. Profiles for 1027 °C (1300 K) and 1077 °C (1350 K) are emphasized using a dashed line and a dotted line, respectively

ratio of integrated intensities for the reflections (111)/(200) and (311)/(222) as a function of temperature. Both ratios seem to be constant below 527 °C (800 K) but increase with temperature in the range 527-727 °C (800-1000 K) and turn to be constant again up to 1027 °C (1300 K). Integration above 1027 °C (1300 K) was not considered because the precision of the intensity ratio is questionable. Since the CsCl phase generally forms preferentially at high temperature, the mixture of two phases will lead to a decrease of the intensity ratios (111)/(200) and (311)/(222) because both intensities (200) and (222) not only benefit from the Heusler phase but also from the CsCl phase. The increase of the intensity ratios shown in Fig. 6 suggests that the CsCl phase does not exist in this temperature range.

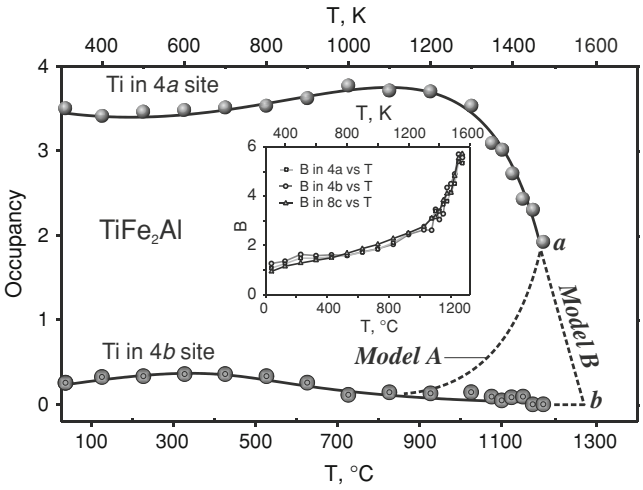

Fig. 7 Occupancy of Ti in 4*a* and 4*b* sites in the alloy $TiFe_2Al$ vs. temperature (details on models A and B are given in the text); inset: temperature dependence of isotropic displacement factors B (Debye-Waller factor) in each site (B given in [100 nm^2])

The atom arrangement in $TiFe_2Al$ as derived from Rietveld refinement of in situ neutron diffraction data shows consistency with that obtained at room temperature. The temperature dependence of the occupancies for Ti in 4*a* and Ti in 4*b* is shown in Fig. 7. As no structural voids were found during the refinements, the temperature dependence of the occupancy for Al in both sites (not shown in Fig. 7) can be easily obtained by subtracting the Ti occupancy from 4. The occupancy of Ti in the 4*a* site is almost constant below 527 °C (800 K) and increases slightly from 527 °C (800 K) to 727 °C (1000 K) but decreases drastically above 1027 °C (1300 K). This trend seems to correspond to that of the intensity ratio (111)/(200) and (311/222) which indicates that the intensities of (111) and (311) reflect the Ti occupancy in 4*a*. Accordingly, at high temperature, the refined compositions of the Heusler phase significantly deviate from the stoichiometric composition $TiFe_2Al$.

The temperature dependence of the site preference for $TiFe_2Al$ (Fig. 7) was analyzed in terms of two boundary models for a possible transformation of the Heusler-type into the CsCl-type structure. As already discussed in Fig. 1, such a transition occurs in case the scattering power of 4*a* and 4*b* sites becomes equivalent. Therefore *model A* would comply with a CsCl-type structure for composition $TiFe_2Al$ at around 1200 °C (point *a*, Fig. 7, $Fe^{8c}(0.5Ti0.5Al)^{4a}(0.5Ti0.5Al)^{4b}$), while the site preference according to *model B* would reveal the CsCl type lattice at ~1300 °C with a composition for binary FeAl (point *b*, $Fe^{8c}Al^{4a}Al^{4b}$, Fig. 7). Attempts to force refinements in *model A* fixing appropriate amounts of Ti in the 4*b* site were ruled out due to high

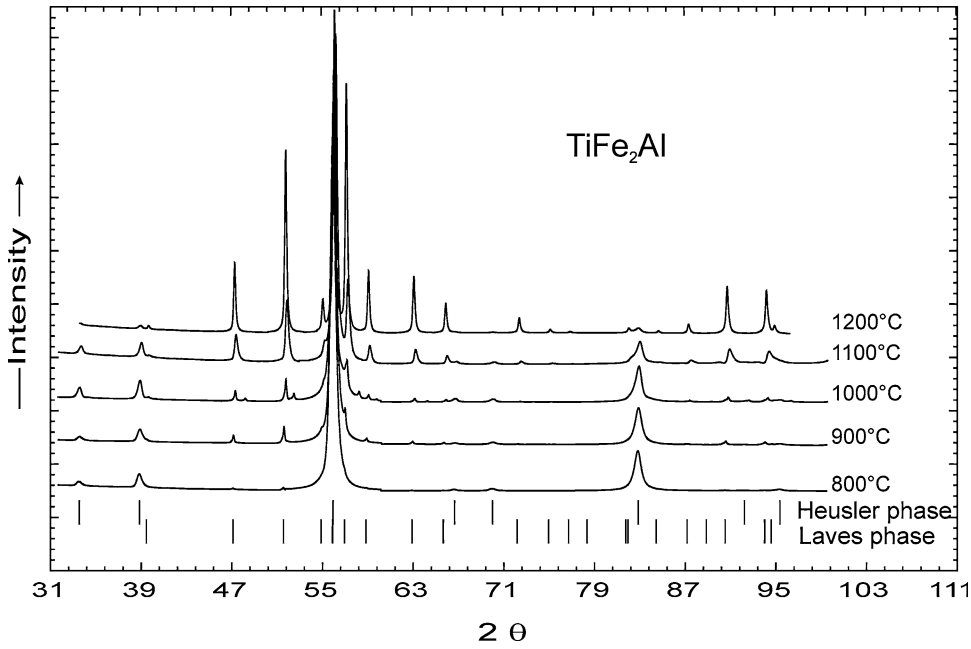

Fig. 8 XPD patterns of $TiFe_2Al$ annealed at various temperatures

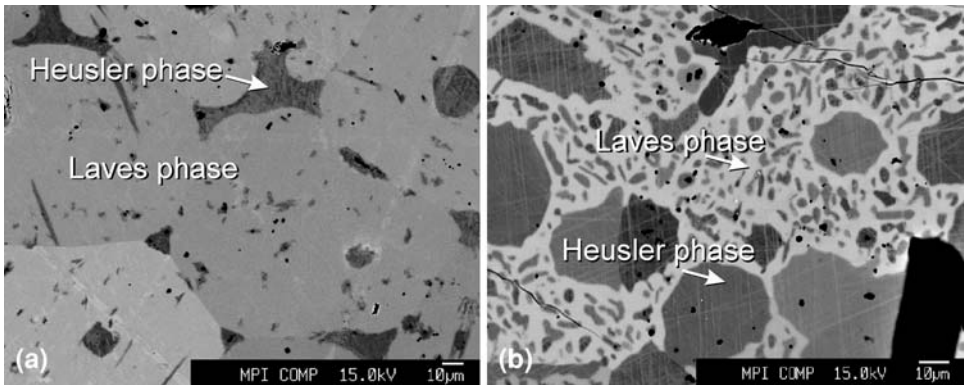

Fig. 9 Microstructures of the alloy $TiFe_2Al$, (a) after neutron diffraction, Laves phase: $Ti_{27.5}Fe_{49.1}Al_{23.4}$, Heusler phase: $Ti_{19.8}Fe_{52.8}Al_{27.4}$; and (b) annealed at 800 °C, Laves phase: $Ti_{28.7}Fe_{48.7}Al_{22.6}$, Heusler phase: $Ti_{23.3}Fe_{51.2}Al_{25.5}$ (data from EPMA in at.%)

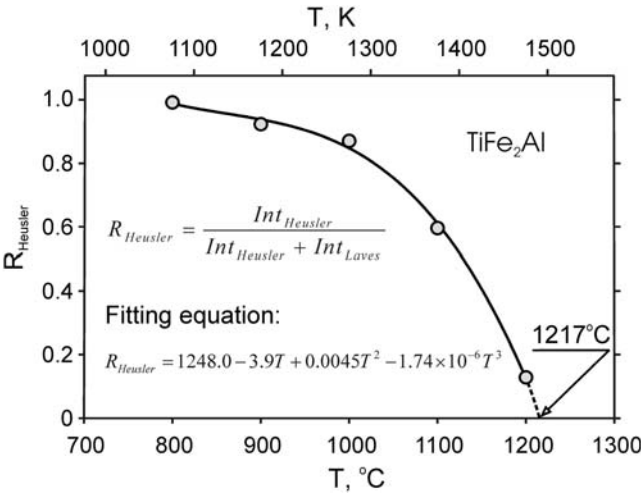

Fig. 10 Fraction of Heusler phase in the alloy $TiFe_2Al$ vs. temperature (data obtained from Rietveld refinement)

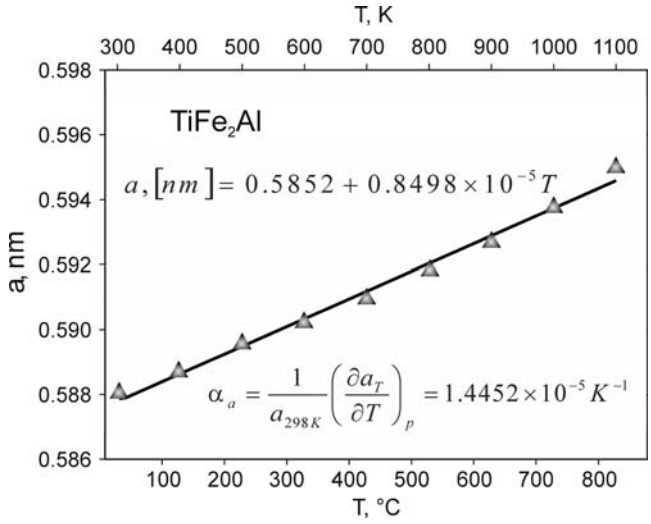

Fig. 11 Thermal expansion coefficient α_a vs. temperature for $TiFe_2Al$

residual values. *Model B* disqualifies by an unacceptable composition (CsCl-type structure only possible at point *b*).

The isotropic displacement factors, B, for all sites in the Heusler unit cell were plotted in Fig. 7(inset) as a function of temperature. A significant rise of B at around 1100 °C indicates the occurrence of a transition. As indicated in Fig. 5, at around this temperature, the amount of Heusler phase in the alloy starts to be reduced greatly on heating.

Analyzing in situ neutron diffraction data we have to consider a slow equilibration rate in the sample at low temperature. One can see from Fig. 5 and 7 that data obtained in the range RT (Room temperature) $< T <$ 900 °C represent almost the same state of the sample, while at higher temperatures significant changes are observed due to an enhanced diffusion rate. In order to elucidate equilibrium conditions for $TiFe_2Al$, the sample was cut into several discs after the neutron diffraction experiment and annealed at various temperatures in the range from 800 to 1200 °C.

The samples after ND diffraction and after annealing at 1200 °C show almost a single Laves phase with a tiny amount of Heusler phase. The volume fraction of the Heusler phase increases with decreasing annealing temperature. Accordingly the sample heat treated at 800 °C reveals major amounts of Heusler phase close to the nominal composition (Fig. 8, 9). The microstructures of the sample after neutron diffraction and after annealing at 800 °C are shown in Fig. 9, indicating an almost single Laves phase at 1277 °C and grain growth and precipitation of Heusler phase after annealing at 800 °C. The ratio of Heusler phase to Laves phase versus annealing temperature is plotted in Fig. 10. A polynomial equation was used to fit the data and an extrapolation derives the threshold temperature as $T = 1217$ °C. It is interesting to note, that this value is close to the temperature, which was interpreted by Ohnuma et al.[16] (from thermal effects) as a structural transformation of $TiFe_2Al$ with Heusler type into CsCl-type. In this context it is important to stress that the $TiFe_2Al$ sample at high temperatures mainly consists of Laves phase in equilibrium with a Ti-depleted Heusler phase $Ti_{\sim 0.5}Fe_2Al_{\sim 1.5}$.

Finally, the thermal expansion coefficient α_a of the Heusler phase $TiFe_2Al$ was calculated through a polynomial fitting of lattice parameters from Rietveld refinements using the relation:

$$\alpha_a = \frac{1}{a_{298\,\mathrm{K}}}\left(\frac{\partial a_\mathrm{T}}{\partial T}\right)_p$$

where α_a is the linear thermal expansion coefficient, $a_{298\ \mathrm{K}}$ is the lattice parameter value at room temperature, and a_T is the lattice parameter value at the measured temperature. Discarding low precision data extracted from the dwindling amount of the Heusler phase at high temperatures, only the lattice parameters below 827 °C (1100 K) were employed for the analysis. The relation of lattice parameter with temperature can be described by a linear equation (see Fig. 11) as: a, nm = $0.5852 + 0.8498\times10^{-6}\ T$. Then $\alpha_a = 1.4552\times10^{-5}\ \mathrm{K}^{-1}$, which is very close to the expansion coefficients of αFe[47,48] and Fe-40 at.% Al (CsCl-type).[49,50]

4. Conclusions

Combined Rietveld refinement of X-ray and neutron diffraction data for $TiFe_2Al$ revealed the structural details of the ternary Heusler phase as a function of temperature and Fe/Ni substitution, i.e., Fe atoms occupy the 8*c* site, Ti with a small amount of Al shares the 4*a* site and the rests of Ti and Al atoms are situated in the 4*a* site. This structural model holds for all alloys $Ti_{25}(Fe_{50-x}Ni_x)Al_{25}$ $(0 \le x \le 50)$ revealing partial order in the Fe-rich side but complete order in the Ni-rich side. Profiles recorded by in situ neutron powder diffraction for $TiFe_2Al$ in the range of investigated temperatures show two phases, namely Heusler phase and $MgZn_2$-type Laves phase. The fraction of Heusler phase in the alloy decreases with temperature. No CsCl-type phase was found in the alloy in the investigated temperature range.

The thermal expansion coefficient of the $TiFe_2Al$ Heusler phase was calculated for the temperature range 300-1100 K (27-827 °C) to be $1.4552\times10^{-5}\ \mathrm{K}^{-1}$.

Acknowledgments

This work was supported by the Austrian National Science Foundation FWF projects no. P16957, P16778 and was partially performed at the Laboratory for Neutron Scattering, ETH Zurich & Paul Scherrer Institut, Nilligen PSI, Switzerland. X. Y. and P. R. are grateful to the OEAD for stipends within the bilateral WTZ Austria-China, project VII.A.16.

References

1. F. Heusler, Ueber Magnetische Manganlegierungen (On Magnetic Manganese Alloys), *Verh. Dtsch. Phys. Ges.*, 1903, **5**, p 219, in German
2. R.S. Polvani, S.T. Wen, and P.R. Strutt, High Temperature Creep in a Semi-Coherent NiAl-Ni2AlTi Alloy, *Metall. Mater. Trans. A*, 1976, **7**(1), p 33-40
3. P.R. Strutt, R.S. Polvani, and J.C. Ingram, Creep Behavior of the Heusler Type Structure Alloy Ni_2AlTi, *Metall. Mater. Trans. A*, 1976, **7**(1), p 23-31
4. M.G. Mendiratta, S.K. Ehlers, and H.A. Lipsitt, DO_3-B2-α Phase Relations in Fe-Al-Ti Alloys, *Metall. Mater. Trans. A*, 1987, **18**, p 509-518
5. R.D. Field, R. Darolia, and D.F. Lahrma, Precipitation in NiAl/Ni_2AlTi Alloys, *Scr. Metall.*, 1989, **23**(9), p 1469-1474
6. W. Lin and A.J. Freeman, Cohesive Properties and Electronic Structure of Heusler $L2_1$-Phase Compounds Ni_2XAl (X=Ti, V, Zr, Nb, Hf, and Ta), *Phy. Rev. B: Condens. Matter.*, 1992, **45**, p 4561-4569
7. Y. Mishima, E.H. Lee, and C.T. Liu, Microstructure, Phase Constitution and Tensile Properties of Co-Ni-Ti-Al Base Multi-Phase Intermetallic Alloys, *Mater. Trans. JIM*, 1995, **36**(8), p 1031-1040
8. U. Prakash and G. Sauthoff, Structure and Properties of Fe-Al-Ti Intermetallic Alloys, *Intermetallics*, 2001, **9**, p 107-112
9. J. Bauer, P. Rogl, A. Pewin, M. Boh, W. Wolf, R. Podloucky, Y. LeFriec, and D. Antoine, TiAl-Based Alloys with Nickel, *Intermetallics*, 1996, **4**, p 71-76
10. P.H. Kitabjian and W.D. Nix, Atomic Size Effects in Ni-Al Based Solid Solutions, *Acta Mater.*, 1998, **46**(2), p 701-710
11. M. Yamaguchi, Y. Umakoshi, and T. Yamane, Plastic Deformation of Ni_2AlTi, *Philos. Mag.*, 1984, **A50**, p 205-220
12. Y. Umakoshi, M. Yamaguchi, and T. Yamane, Effects of Non-Stoichiometry on the High-Temperature Deformation of Ni_2AlTi, *Philos. Mag.*, 1985, **A52**, p 357-367
13. C.T. Liu, C.L. White, and J.A. Horton, Effect of Boron on Grain-Boundaries in Ni_3Al, *Acta Metall.*, 1985, **33**, p 213
14. G. Bozzolo, R. Noebe, J. Ferrante, A. Garg, F. Hongecy, and C. Amador, BFS Simulation and Experimental Analysis of the Effect of Ti Additions on the Structure of NiAl, *J. Comput. Aided Mater. Des.*, 1999, **6**, p 33-68
15. R. Kainuma, K. Urushiyama, K. Ishikawa, C.C. Jia, I. Ohnuma, and K. Ishida, Ordering and Phase Separation in b.c.c. Aluminides of the Ni-Fe-Al-Ti System, *Mater. Sci. Eng., A*, 1997, **239-240**, p 235-244
16. I. Ohnuma, C.G. Schön, R. Kainuma, G. Inden, and K. Ishida, Ordering and Phase Separation in the b.c.c. Phase of the Fe-Al-Ti System, *Acta Mater.*, 1998, **46**(6), p 2083-2091
17. R. Ducher, "Contribution à l'étude du diagramme de phase ternaire Fe-Ti-Al et des équilibres Fe-TiAl," Dr. Thesis, ENSIACET Toulouse, 2003, p 1-171
18. W.J. Boettinger, L.A. Bendersky, F.S. Biancaniello, and J.W. Cahn, Rapid Solidification and Ordering of B2 and $L2_1$ Phases in the NiAl-NiTi System, *Mater. Sci. Eng.*, 1988, **98**, p 273-276
19. J. Jung, G. Ghosh, and G.B. Olson, A Comparative Study of Precipitation Behavior of Heusler Phase (Ni_2TiAl) from B2-TiNi in Ni–Ti–Al and Ni–Ti–Al–X (X = Hf, Pd, Pt, Zr) Alloys, *Acta Mater.*, 2003, **51**, p 6341-6357

20. M. Enomoto and T. Kumeta, Analysis of the β' $Ni_2TiAl/\beta NiTi$ Equilibrium in Ni-Ti-Al Alloys by the Cluster Variation Method, *Intermetallics*, 1997, **5**, p 103-109
21. K. Ishikawa, H. Mitsui, I. Ohnuma, R. Kainuma, K. Aoki, and K. Ishida, Ordering and Phase Separation of BCC Aluminides in (Ni, Co)-Al-Ti System, *Mater. Sci. Eng., A*, 2002, **329-331**, p 276-281
22. K. Ishikawa, R. Kainuma, I. Ohnuma, K. Aoki, and K. Ishida, Phase Stability of the X_2AlTi (X: Fe, Co, Ni and Cu) Heusler and B2-Type Intermetallic Compounds, *Acta Mater.*, 2002, **50**, p 2233-2243
23. K. Ishikawa, I. Ohnuma, R. Kainuma, K. Aoki, and K. Ishida, Phase Equilibria and Stability of Heusler-Type Aluminides in the $NiAl–Ni_2AlTi–Ni_2AlY$ (Y: V, Cr or Mn) System, *J. Alloys Compd.*, 2004, **367**, p 2-9
24. A.W. Wilson and J.M. Howe, Effect of Alloying Additions on β′ Precipitation in NiAl-Ti Base Alloys, *Acta Mater.*, 2001, **49**, p 2653-2660
25. G. Bozzolo, R.D. Noebe, J. Ferrante, and A. Garg, Atomistic Simulations of Alloying Additions to NiAl, *Mater. Sci. Eng., A*, 1997, **239-240**, p 769-776
26. Y. Nishino, C. Kumada, and S. Asano, Phase Stability of Fe_3Al with Addition of 3d Transition Elements, *Scr. Mater.*, 1997, **36**(4), p 461-466
27. S.K. Ehlers and M.G. Mendiratta, Tensile Behaviour of Two DO_3-Ordered: Fe_3Si and Fe-20 at% Al-5 at% Si, *J. Mater. Sci.*, 1984, **19**, p 2203-2210
28. Y. Nishino, Electrical Resistance Anomaly in Fe_3Al-Based Alloys, *Mater. Sci. Eng., A*, 1998, **258**, p 50-58
29. J.G. Cabañas-Moreno, T. Itsukaichi, and M. Umemoto, A New Phase in Al-Ni-Ti Alloys Made from Mechanically Alloyed Powders, *Mater. Sci. Eng., A*, 1994, **181-182**, p 1202-1206
30. S.H. Mahmood, M.A. Gharaibeh, and A.S. Saleh, Mössbauer and Structural Studies of $FeAl_{1-x}Ti_x$, *Solid State Commun.*, 1995, **95**(4), p 263-266
31. P.O. Suzuki and T. Kyono, Thermoelectric Properties of Fe_2TiAl Heusler Alloys, *J Alloys Compd.*, 2004, **377**, p 38-42
32. W.B. Pearson, Chapter II: Tabulated Lattice Parameters and Data on Elemental Metals and Metalloids, *Handbook of Lattice Spacings and Structures of Metals*, 2nd ed., W.B. Pearson, Ed. (New York), Pergamon Press, 1967, p 127
33. A.E. Dwight, Body-Centered Cubic Derivative Structures, *Intermetallic Compounds*, J.H. Westbrook Ed. (New York), Wiley Press, 1967, p 174
34. P.D. Parsons and J. Nutting, Electron Metallography of an Austentic Steel Containing Aluminal and Titanium, *J. Iron Steel Inst.*, 1969, **207**, p 230
35. K.H.J. Buschow and P.G. Van Engen, Magnetic and Magneto-Optical Properties of Heusler Alloys Based on Aluminum and Gallium, *J. Magn. Magn. Mater.*, 1981, **25**, p 90-96
36. S. Sridharan, H. Nowotny, and S.F. Wayne, Investigations within the Quaternary System Titanium-Nickel-Aluminium-Carbon, *Monatsh. Chem.*, 1983, **114**, p 127-135
37. K.H.J. Buschow, P.G. Van Engen, and R. Jongebreur, Magneto-Optical Properties of Metallic Ferromagnetic Materials, *J. Magn. Magn. Mater.*, 1983, **38**, p 1-22
38. D.E. Okpalugo, J.G. Booth, and C.A. Faunce, Onset of Ferromagnetism in 3d-Substituted FeAl Alloys. I: Ti, V and Cr Substitution, *J. Phys. F: Metal Phys.*, 1985, **15**, p 681-692
39. B. Huneau, P. Rogl, K. Zeng, R. Schmid-Fetzer, M. Bohn, and J. Bauer, The Ternary System Al-Ni-Ti Part I: Isothermal Section at 900°C: Experimental Investigation and Thermodynamic Calculation, *Intermetallics*, 1999, **7**, p 1337-1345
40. F.S. da Rocha, G.L.F. Fraga, D.E. Brandão, C.M. da Silva, and A.A. Gomes, Specific Heat and Electronic Structure of Heusler Compounds Ni_2TAl (T=Ti, Zr, Hf, V, Nb, Ta), *Physica B*, 1999, **269**, p 154-162
41. H. Fu, D. Chen, X. Cheng, T. Gao, and X. Yang, The Influence of the X Atoms and Al 3p Occupied States in $AlTiX_2$ (X = Fe, Cu, Co, Ni), *Physica B*, 2007, **388**, p 303-311
42. P. Fischer, G. Frey, M. Koch, M. Koennecke, V. Pomjakushin, J. Schefer, R. Thut, N. Schlumpf, R. Buerge, U. Greuter, S. Bondt, and E. Berruyer, High-Resolution Powder Diffractiometer HRPT for Thermal Neutrons at SINQ, *Physica B*, 2000, **276-278**, p 146-147
43. T. Roisnel and J. Rodríquez-Carvajal, WinPLOTR: A Windows Tool for Powder Diffraction Pattern Analysis, *Mater. Sci. Forum*, 2001, **378-381**, p 118
44. M. Palm, G. Inden, and N. Thomas, The Fe-Al-Ti System, *J. Phase Equilb.*, 1995, **16**, p 209-222
45. M. Palm and J. Lacaze, Assessment of the Al-Fe-Ti System, *Intermetallics*, 2006, **14**, p 1291-1303
46. E. Parthé, L. Gelato, B. Chabot, M. Penzo, K. Cenzual, and R. Gladyshevskii, TYPIX Standardized Data and Crystal Chemical Characterization of Inorganic Structure Types, *Gmelin Handbook of Inorganic and Organometallic Chemistry*, 8th ed. (Berlin), Springer-Verlag, 1994
47. C.Y. Ho, Thermal Expansion of Solids, *CINDAS Data Series on Material Properties*, Vol. 1-4 (Ohio), ASM International, 1998
48. N.A. Dubrovinskaia, L.S. Dubrovinsky, A. Karisson, and S.K. Saxena, Experimental Study of Thermal Expansion and Phase Transformations in Iron-Rich Fe-Al Alloys, *CALPHAD*, 1999, **23**(1), p 69-84
49. B.V. Reddy and S.C. Deevi, Thermophysical Properties of FeAl (Fe-40 at.%Al), *Intermetallics*, 2000, **8**, p 1369-1376
50. S.C. Deevi, Powder Processing of FeAl Sheets by Roll Compaction, *Intermetallics*, 2000, **8**, p 679-685